Andrij MILENIN [0000-0002-6266-2881]*

PARALLEL SOLUTION OF THERMOMECHANICAL INVERSE PROBLEMS FOR LASER DIELESS DRAWING OF ULTRA-THIN WIRE

Abstract

The paper discusses the solving of inverse thermomechanical problems requiring a large number of FEM tasks with various boundary conditions. The study examined the case when all tasks have the same number of nodes, finite elements, and nodal connections. In this study, the speedup of the solution of the inverse problem is achieved in two ways: 1. The solution of all FEM tasks in parallel mode. 2. The use by all FEM tasks a common matrix with addresses of nonzero elements in the stiffness matrices. These algorithms are implemented in the own FEM code, designed to solve inverse problems of the hot metal forming. The calculations showed that developed code in parallel mode is effective for the number of tasks late than 0,7-0,9 of the number of available processors. Thus, at some point, it becomes effective to use a sequential solution to all tasks and to use a common matrix of addresses of nonzero elements in the stiffness matrix. The achieved acceleration at the optimal choice of the algorithm is 2–10 times compared with the classical multivariate calculations in the FEM. The paper provides an example of the practical application of the developed code for calculating the allowable processing maps for laser dieless drawing of ultra-thin wire from copper alloy by solving the thermomechanical inverse problem. The achieved acceleration made it possible to use the developed parallel code in the control software of the laboratory setup for laser dieless drawing.

1. INTRODUCTION

Inverse thermomechanical problems arise when the subject of analysis is both the mechanical behavior of the material (Kubo, 1988) and the temperature distribution (Jaluria, 2021). Such problems are often encountered in technical applications of theories of elasticity, fluid mechanics, plasticity, and heat transfer (Lesnic, 2021). A rather difficult version of these problems is associated with the hot metal forming (Chenot, Massoni & Fourment, 1996). In this case, the direct problem contains the coupled problems of unsteady-state heat transfer and deformation of an incompressible viscoplastic material. One of the well-known inverse problems in practice is to determine the parameters of a material model based on indirect experimental data. For example, in the paper (Szeliga & Pietrzyk, 2007) the problem of determining the flow stress model of microalloyed niobium steel was considered.

---

* AGH University of Science and Technology, Faculty of Metals Engineering and Industrial Computer Science, Department of Applied Computer Science and Modelling, Krakow, Poland, milenin@agh.edu.pl

As the objective function, the square of the difference between the experimental results (for example, the compression force in the plastometric test) and the FEM calculation is used. As shown in (Szeliga, Gawąd & Pietrzyk, 2004), the optimization method is essential. This is because the inverse analysis requires a large number of similar FEM tasks, especially when identifying complex materials (Pokorska, 2007). Another type of inverse problems is associated with the determination of process parameters that lead to a given result – for example, to the necessary metal forming (Thomas et al., 2017). An interesting example in this sense is the relatively new process of laser dieless drawing of thin wire. The process of laser dieless drawing is a stretching of a wire with its simultaneous local heating in the deformation zone by a laser beam (Li, Quick & Kar, 2002). This process differs significantly from the conventional wire drawing. The conventional process is based on a drawing in dies with diamond cores. The use of a die significantly increases the cost of the process. Also, conventional wire drawing requires the use of some lubricants, and their chemical removal from the final wire degrades the surface quality and is not harmless to the natural environment. Thus, conventional technology is quite expensive (Kraft, 1980). On the other hand, in laser dieless drawing, the prediction of such parameters as the final wire diameter, strain, or temperature of the deformation requires complex FEM calculations. It is important to note that because of the asymmetry of laser heating, the boundary value problem becomes three-dimensional. For this reason, the existing axisymmetric FEM solutions for typical dieless drawing process with electrical or induction heating (for example (Furushima & Manabe, 2007) or (Tiernan & Hillery, 2004)) cannot be applied.

In the dieless drawing process, the diameter of the wire is formed freely and is not determined by the shape of the die, in contrast to conventional wire drawing (Tiernan & Hillery, 2008). Thus, to determine the laser dieless drawing parameters leading to the production of a wire of a given diameter, the inverse problem must be solved. Furthermore, from this point of view, solving the individual direct problem for this process is usually not of practical interest. This is the first important feature of this process. The second feature of the laser dieless drawing of thin wire is the practical need to obtain a map of allowable process parameters. To compile such a map, it is necessary not only to find the one optimal solution but also to solve the vector of direct problems. Solving the inverse problem in such a formulation requires a significant speedup of the numerical solution by optimizing the FEM code. The third feature of the process is that all FEM tasks have the same number of nodes, finite elements, and same nodal connections (in this process is not necessary of remeshing of FEM grid during the calculation). This means that the position of nonzero elements in the stiffness matrix is the same for all tasks, solved in the process of inverse analysis. Thus, considering the solution of the inverse problem as the main mode of operation of the developed FEM code, the address matrix of nonzero elements of the stiffness matrices (thermal and mechanical) can be determined once and used by all FEM tasks during the inverse analysis.

The second way to speed up the solution of the inverse problem is to use parallel computing. The idea of using parallel computing to solve inverse problems was applied earlier, for example, in (Milenin, 2017) to analyze tube production by laser dieless drawing. A comparison of the results of the calculation of temperature and strain with experimental data showed their good agreement (Milenin et al., 2018). However, these findings cannot be extrapolated directly to laser drawing of thin wire because in this process the FEM grid and stiffness matrices had a different structure. On the other side, recent research (Milenin,

Wróbel & Kustra, 2022) has suggested that during the production of thin wire by dieless drawing the use of such FEM code for analysis and optimizing the production parameters is much more important, since experimental control of the temperature and deformation of a wire with a diameter of several tens of micrometers is very difficult.

Thus, in this paper, the FEM code for solving inverse problems based on the use of both a general address matrix of nonzero elements of stiffness matrices and parallel computations is proposed for laser dieless drawing of thin wire. The paper also investigates the numerical efficiency of the developed code using the example of the laser dieless drawing problem of a thin wire made of CuZn37 alloy. The paper also proposes a practical solution to the inverse problem in the form of an allowable processing map.

2. FEM MODEL OF THE LASER DIELESS DRAWING PROCESS OF WIRE

2.1. Description of the laser dieless drawing process of thin wire

The process of elongation of the wire during the laser dieless drawing takes place in a small volume of material heated by a laser beam with a diameter of 0.4 mm. In Fig. 1 this corresponds to the intersection of beam 4 with wire 1. The rollers of the drawing machine rotate at different speeds, with $V_1 > V_0$. The larger the value of $\Delta V = V_1 - V_0$, corresponding to the greater elongation of the wire. However, a too large ΔV value will lead to wire breakage. The deformation temperature also depends on the velocities V_1, V_0. The higher velocities, the shorter the heating time of the wire and the lower the deformation temperature. Since the laser heats the wire only on one side, the task is three-dimensional. Only the part of the wire that is near the heating zone is considered during FEM simulation.
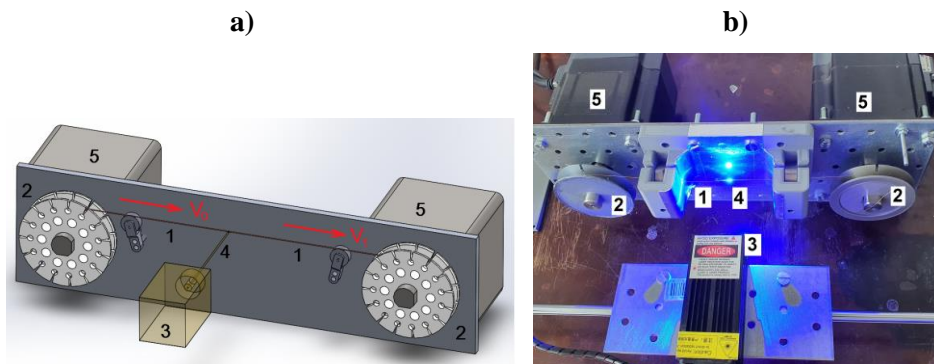
a) **b)**

Fig. 1. Scheme (a) and the corresponded setup (b) of the simulated process: 1 – wire; 2 – rollers; 3 – laser; 4 – laser beam; 5 – engines

2.2. FEM model

The boundary problem is described by the equations of the theory of plasticity for non-compressible materials and the equation of non-steady-state heat exchange. In this model the flow velocities v_i, the mean stress σ_0 and temperature t is unknown. Thus, the developed FEM code contains the solution of the following group of equations:

- equilibrium equations:

$$\sigma_{ij,i} = 0,\tag{1}$$

- compatibility condition:

$$\dot{\varepsilon}_{ij} = \frac{1}{2}\left(v_{i,j} + v_{j,i}\right),\tag{2}$$

- constitutive equations:

$$\sigma_{ij} = \delta_{ij}\sigma_0 + \frac{2\sigma}{3\dot{\varepsilon}}\dot{\varepsilon}_{ij},\tag{3}$$

- incompressibility equation:

$$v_{i,j} = 0,\tag{4}$$

- equation of non-steady state heat exchange:

$$\rho c \dot{t} = div\big(k\ grad(t)\big) + \beta\sigma\dot{\varepsilon},\tag{5}$$

- and model for flow stress:

$$\sigma = \sigma(\varepsilon, \dot{\varepsilon}, t),\tag{6}$$

where: σ_{ij} – stress tensor,
σ_0 – mean stress,
$\dot{\varepsilon}_{ij}$ – strain rate tensor,
v_i – velocity component,
$\sigma, \varepsilon, \dot{\varepsilon}$ – flow stress, effective strain, and effective strain rate, respectively,
t – temperature,
β – heat generation efficiency which is usually assumed as $\beta = 0.95$,
k – thermal conductivity,
ρ – density,
c – heat capacity.

In equations (1)–(5) summation convention is used.

As a model for flow stress (6) the equation of Hensel-Spittel (Hensel & Spittel, 1978) was used:

$$\sigma = A\ exp(m_1 t)\varepsilon^{m_2}\dot{\varepsilon}^{m_3}exp(m_4/\varepsilon)(1+\varepsilon)^{m_5 t}exp(m_6\varepsilon)\ \dot{\varepsilon}^{m_7 t}\ t^{m_8}\tag{7}$$

Following empirical coefficients A and $m_1 - m_8$ for CuZn37 alloy have been found in the paper (Milenin et al., 2022) as a result of the inverse analysis of the plastometric tests: $A = 81259.14$, $m_1 = -0.004279279$, $m_2 = 0.09383521$, $m_3 = -0.03657546$, $m_4 = -0.004250721$, $m_5 = 6.06186E{-}05$, $m_6 = -0.4821499$, $m_7 = 0.000317437$, $m_8 = -0.596443559$.

Equations (1)–(4) were transformed into the discrete form using the virtual work-rate principle and FEM technique resulting in a linear system of algebraic equations. The equation of non-steady-state heat exchange (5) is treated using the Galerkin method.

The mechanical boundary conditions involve moving and tensile of wire along heated zone according to the scheme in Fig. 1. The thermal boundary conditions on the contact of wire with air are described by the convection law:

$$q_{air} = \alpha_{air}(t - t_{\infty}) \tag{8}$$

and for heating zone are presented in the form of heat flux:

$$q_{laser} = A\frac{W}{S} \tag{9}$$

where: W – laser power (5.5 W),
A – absorption coefficient of the laser (0.91),
S – the area of contact between the laser and the wire,
α_{air} – coefficient of convective heat exchange with air (120 W/^{0}C m^2),
t_{∞} – the temperature of the environment (20 ^{0}C).

The 8-nodal 3d isoparametric finite elements were used.

2.3. Properties of matrices (using a shared address matrix)

Consider the properties of the stiffness matrix for a mechanical problem. For the heat capacity matrix for the thermal problem, the conclusions are similar. The global stiffness matrix after assembling is sparse. For the grid chosen as an example (12288 nodes, 9155 elements, 46019 Degree Of Freedom (DOF)) there is 0.14% of the non-zero elements in the global stiffness matrix for the mechanical problem and 0.18% for the thermal problem. A schematic representation of the positions of nonzero elements in the heat capacity matrix and stiffness matrix is presented in Fig. 2, a and Fig. 2, b respectively. For such systems of equations, a solver for sparse matrix should be used. In this study, PARDISO software presented by (Schenk & Gärtner, 2004) was used.

a)   b)
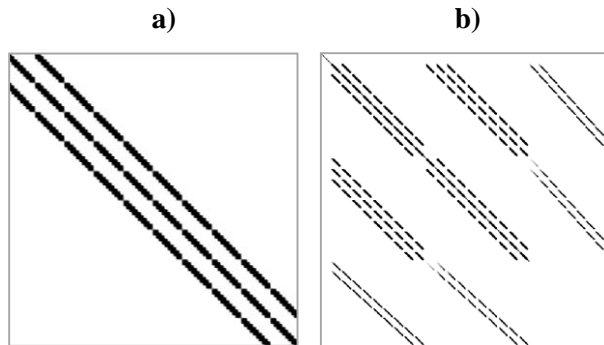
**Fig. 2. Graphic representation of heat capacity (a) and stiffness matrices (b);
black pixels – nonzero values, white pixels – zero values**

For solving systems of equations the following data have to be transmitted to PARDISO solver:

– the number of nonzero elements in the stiffness matrix (*Nonzero*);
– nonzero values in a stiffness matrix (*AK*(*Nonzero*));
– the number of column in the full stiffness matrix containing the nonzero values *JA*(*Nonzero*);
– the beginning of each row *IA*(DOF+1). *IA*(*i*) points to the first column index of row *i* in the array *JA* in compressed sparse row format, *IA*(DOF+1) = *Nonzero* + 1.

The process of solving the system of equations for one time step is relatively fast (is 16 seconds for *DOF* = 46019), but the preparation of the above data requires much more time (is 132 seconds).

One of the key ideas of the proposed solution is to use the fact that for a one task arrays *JA* and *IA* remain constant at every time step. Thus, the task is to find quickly the position of the coefficients of the global stiffness matrix in the linear array *AK*. The proposed solution is to form a service matrix of indexes *IJ*(DOF,DOF) containing an integer number of non-zero elements in *AK* array. For zero elements of the stiffness matrix, *IJ* contains 0. Thus, it is possible to directly fill an array *AK* during assembling the elements. The memory of matrix *IJ*(DOF,DOF) for the described example is more than 8 Gb. This is still a large amount of data, but it is filled once and does not change in the process of the solution. Essential is also the fact that it is possible to use the same copy of the array *IJ* for all tasks solved in the parallel mode. In that case, the proposed solution becomes more efficient both for parallel and sequential solutions of the tasks vector.

2.4. Example of simulation

An example of the simulation result of the direct problem is shown in Fig. 3 and Fig. 4. For this example $V_0 = 15$ mm/s, $V_1 = 20$ mm/s. The top image in Fig. 3 corresponds to one of the intermediate stages of the calculation, the bottom – to the last. As follows from the distributions in Fig. 3, the maximum temperature is localized over a very short wire length (about 0.5 mm), which leads to a high strain rate (Fig. 4).
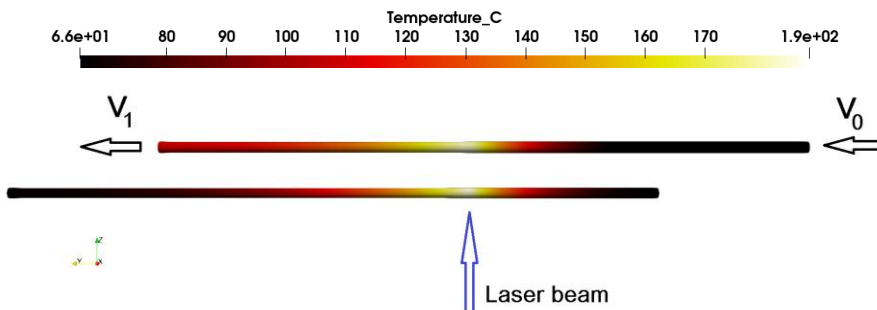
Fig. 3. An example of the result of temperature calculation for the initial (top) and final (down) moment of the simulation
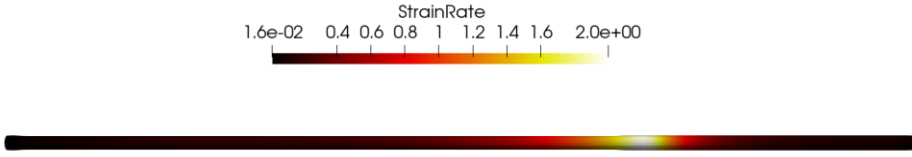
Fig. 4. An example of the result of the strain rate calculation

2.6. Parallelization

The identical numbers of nodes, elements, and same nodal connections for all used FE grids guarantee the same position of non-zero elements in the global stiffness matrix. Therefore, arrays *IA*, *JA*, and *IJ* for all tasks at all stages of the solutions will be the same and can be stored in a single copy. Thus, only the organization of the access to these data to all parallel processes is needed. OpenMP library (Chandra et al., 2001) is used to implement a parallel FEM code. In each parallel task, the sequential algorithm of FEM calculation was used. That's why each task used only one processor and the number of used processors is equal to the number of tasks (*N*). The developed code automatically distributes the processors after generating the vector of tasks. All calculations were performed on Intel® Workstation with Xeon® 2.27 GHz 16-cores processor and 24 GB RAM.

3. RESULTS

In the developed code speedup of calculations is achieved in two independent ways. The first is based on one calculation of one index matrix *IJ*(DOF,DOF) for all tasks. The effectiveness of this method depends on the relationship between the time of calculating the index matrix IJ τ_m and the time of one solution of FEM τ_S. During calculation, the number of tasks N variated from 1 to 20. The calculations were performed on a computer with the number of processors (*p*) 16.

For conventional sequential computations, the calculating time is $\tau = N(\tau_m + \tau_S)$. But if the proposed algorithm is used, this value becomes equal to $\tau = \tau_m + N\tau_S$. Therefore, $SpeedUp_1$ can be calculated from the equation:

$$SpeedUp_1 = \frac{(\tau_S + \tau_m)N}{\tau_m + N\tau_S} \tag{10}$$

The value of $SpeedUp_1$ depends on DOF, *N,* and conditions of calculation. For the analysis, three FEM models with different DOF in mechanical tasks were chosen. Model 1 matched the DOF = 23004, model 2 – DOF = 46008, and model 3 – DOF = 60963. The dependence of $SpeedUp_1$ on the number of tasks (*N*) and the value of DOF is shown in Fig. 5.
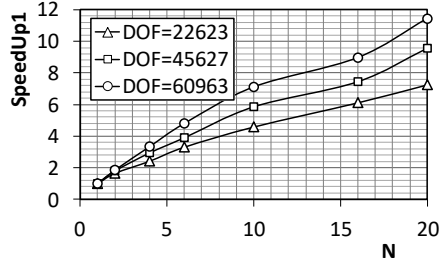
**Fig. 5. Dependence of *SpeedUp1* on the number of tasks (N)
and the value of the degree of freedom (DOF)**

The second way of speedup computing is based on the parallelization of calculations. To evaluate the efficiency of parallel computations, a comparison was made between parallel and sequential modes. The two parameters were calculated to evaluate the efficiency of parallel computations:

$$SpeedUp_2 = \frac{(\tau_s + \tau_m)N}{\tau_m + \tau_{sNpar}} \tag{11}$$

and

$$SpeedUp_3 = \frac{\tau_s N}{\tau_{sNpar}} \tag{12}$$

where: τ_{sNpar} – time of solution of *N* tasks in parallel mode.

The parameter *SpeedUp2* characterizes the total acceleration of the solution from the influence of two factors – the use of a common matrix of addresses of nonzero elements and parallel solution of FEM tasks. Fig. 6 shows the dependence of *SpeedUp2* on *N*. Unlike *SpeedUp1*, the dependence of *SpeedUp2* on *N* is non-linear and has an extremum for large DOF. The reasons for this nonlinearity will become clear if we analyze the dependence of *SpeedUp3* on N (Fig. 7). As follows from Fig. 7, the speedup during solving the FEM tasks in parallel mode decreases to 1 at *N* = 11–15.
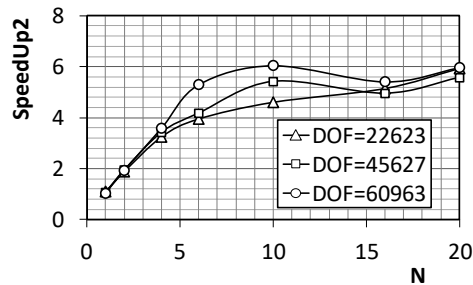
**Fig. 6. Dependence of SpeedUp2 on the number of tasks (N)
and the value of the degree of freedom (DOF)**

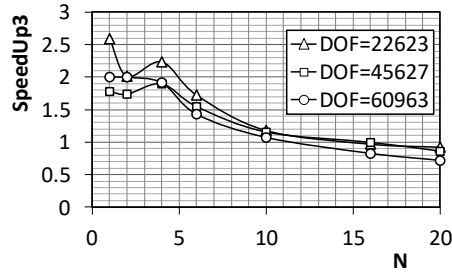**Fig. 7. Dependence of SpeedUp₃ on the number of tasks (N)
and the value of the degree of freedom (DOF)**

4. DISCUSSION AND PRACTICAL IMPLEMENTATION

The calculation results showed that the speedup of parallel solution (*SpeedUp₃*) decreases with an increase in the number of parallel tasks (parallel slowdown). This is because the number of calls to one common piece of computer memory (matrix with addresses of nonzero elements in the stiffness matrix) is increasing. There is also a decrease in *SpeedUp₃* when the number of tasks exceeds the number of available processors. It is empirically established that developed code in parallel mode is effective for number of tasks late than 0,7–0,9 of the number of available processors. Thus, at some point, it becomes effective to use a sequential solution to all tasks and to use a shared matrix of addresses of nonzero elements in the stiffness matrix. The achieved acceleration at the optimal choice of the algorithm is 2–10 times compared with the classical multivariate calculations in the FEM. For sequential mode the dependence between the time of solution and N is close to linear for all ranges of N. However for parallel mode, this dependence is not linear. The time of solution in parallel mode significantly increased for $N > p$ and became more than the time of sequential solution (*SpeedUp₃* < 1).

Consider the practical application of the developed code to obtain a map of allowable parameters. To this goal, we perform calculations by the technique of the factor design. Velocity V_0 varied in the range 10–20 mm/s with increments of 5 mm/s, and ΔV varied in the range 2–11 mm/s with increments of 3 mm/s. Such a matrix of factors led to the calculation of 12 variants. The initial diameter of the wire was 0.2 mm, the laser power was 5.5 W and the diameter of the laser beam was 0.4 mm. This value is larger than the wire diameter. Therefore, only part of the laser energy heats the wire. This fact was taken into account in the model by determining the real area of intersection of the laser beam and the wire. The results of calculating the final diameter are presented in the form of a map of allowable parameters (Fig. 8). On this map, the isolines correspond to the final diameter of the wire, which can be obtained using the appropriate combination ΔV and V_0. The area above the isoline 0.1 mm corresponds to the neck formation and subsequent breaking of wire (in Fig. 8 it is indicated by the caption "Fracture"). An example of a calculation in which a neck is formed is shown in Fig. 9. Thus, the resulting map allows to determine the process parameters based on the required final wire diameter, that is, solve the inverse problem. The solution was carried out in parallel mode, the total solution time was 2h 15'. The achieved speedup of calculation of inverse problems made it possible to use the developed FEM code in the control software of laboratory setup for laser dieless drawing, shown in Fig. 1 for generation maps of allowable parameters for required diameters and materials.

50
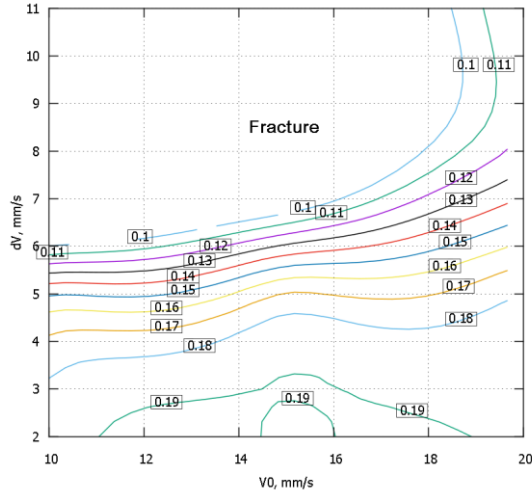
Fig. 8. Calculated allowable processing map for laser dieless drawing of wire from CuZn37 alloy for initial wire diameter 0.2 mm

Experimental tests, carried out on a laboratory setup (Fig. 1, b) in accordance with the calculated allowable processing map (Fig. 8) showed the following. For the calculation shown in Fig. 9, a, in the experiment, a wire breakage is also observed according to the neck formation mechanism (Fig. 9, b).

On the other hand, drawing in the zone of acceptable parameters gives a satisfactory result, which consists in obtaining a defect-free wire, which is shown in Fig. 10.

a)

b)
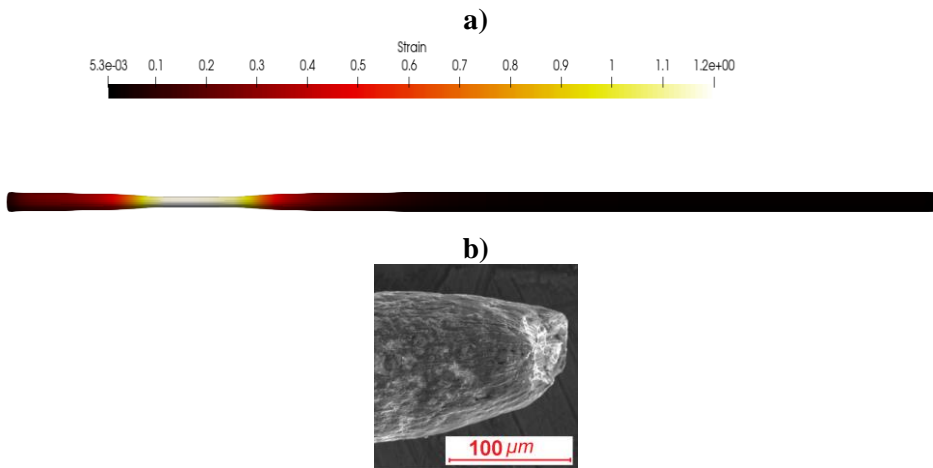
Fig. 9. Example of neck formation during dieless drawing ($V_0 = 15$ mm/s, $\Delta V = 7$ mm/s): a – simulation; b – experiment

a) **b)**
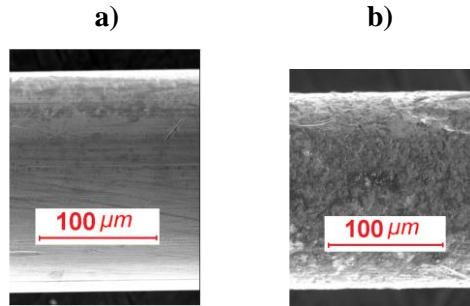
Fig. 10. Example of successive deformation of wire according allowable processing map
(V_0 = 15 mm/s, ΔV = 5 mm/s): a – initial wire of diameter 0.2 mm; b – wire after dieless drawing
to diameter 0.17 mm

5. CONCLUSIONS

This study is devoted to the problem of solving and accelerating the solution of inverse thermomechanical problems for the laser dieless drawing process of thin wire. The proposed methods, however, can be extended to any inverse problems, when all direct tasks have the same number of nodes, finite elements, and same nodal connections.

The developed FEM code was designed to solve inverse problems in the technology of laser dieless drawing of thin wires. The numerical efficiency of the code is based on simultaneous use by all FEM tasks one shared matrix of addresses of non-zero elements in the stiffness matrix and parallel computing. The developed FEM code in parallel mode is more effective for the number of tasks late than 0.7-0.9 of the number of available processors.

A practical example of analysis of the laser dieless drawing process, in which the map of allowable parameters was obtained, is shown and validated in the study.

REFERENCES

Chandra, R., Dagum, L., Kohr, D., Menon, R., Maydan, D., & McDonald, J. (2001). *Parallel Programming in OpenMP*. Elsevier Science.

Chenot, J., Massoni, E., & Fourment, J. L. (1996). Inverse problems in finite element simulation of metal forming processes. *Engineering Computations*, *13*(2/3/4), 190–225. https://doi.org/10.1108/02644409610114530

Furushima, T., & Manabe, K. (2007). Experimental and numerical study on deformation behavior in dieless drawing process of superplastic microtubes. *Journal of Materials Processing Technology*, *191*(1), 59–63. https://doi.org/https://doi.org/10.1016/j.jmatprotec.2007.03.084

Hensel, A. & Spittel, T. (1978). *Kraft- und Arbeitsbedarf bildsamer Formgebungsverfahren*. VEB Deutscher Verlag fur Grundstoffindustrie.

Jaluria, Y. (2021). Strategies for solving inverse problems in thermal processes and systems. *International Journal of Numerical Methods for Heat & Fluid Flow*, *31*(10), 3073–3088. https://doi.org/10.1108/HFF-12-2019-0926

Kraft, F. B. (1980). Three fine wire drawing systems – in economic comparison. *Wire Journal International*, *19*, 103–105.

Kubo, S. (1988). Inverse Problems Related to the Mechanics and Fracture of Solids and Structures. *JSME International Journal. Ser. 1, Solid Mechanics, Strength of Materials*, *31*(2), 157–166. https://doi.org/10.1299/jsmea1988.31.2_157

Lesnic, D. (2021). *Inverse Problems with Applications in Science and Engineering*. Chapman and Hall/CRC.

Li, Y., Quick, N. R., & Kar, A. (2002). Dieless laser drawing of fine metal wires. *Journal of Materials Processing Tech.*, *123*(3), 451–458.

Milenin, A. (2017). Parallel FEM code for simulation of laser dieless drawing process of tubes. *Computer Methods in Materials Science*, *17*(4), 178–185.

Milenin, A., Kustra, P., Furushima, T., Du, P., & Němeček, J. (2018). Design of the laser dieless drawing process of tubes from magnesium alloy using FEM model. *Journal of Materials Processing Technology*, *262*, 65–74. https://doi.org/https://doi.org/10.1016/j.jmatprotec.2018.06.018

Milenin, A., Wróbel, M., & Kustra, P. (2021). Investigation of the workability and surface roughness of thin brass wires in various dieless drawing technologies. *Archives of Civil and Mechanical Engineering*, *22*(1), 10. https://doi.org/10.1007/s43452-021-00331-2

Pokorska, I. (2007). Direct and inverse problems in metal forming of rigid-poroplastic materials. *Journal of Materials Processing Technology*, *184*(1), 146–156. https://doi.org/https://doi.org/10.1016/j.jmatprotec.2006.11.015

Schenk, O., & Gärtner, K. (2004). Solving unsymmetric sparse systems of linear equations with PARDISO. *Future Generation Computer Systems*, *20*(3), 475–487. https://doi.org/https://doi.org/10.1016/j.future.2003.07.011

Szeliga, D., Gawąd, J., & Pietrzyk, M. (2004). Parameters Identification of Material Models Based on the Inverse Analysis. *International Journal of Applied Mathematics and Computer Science*, *14*, 549–556.

Szeliga, D., & Pietrzyk, M. (2007). Testing of the inverse software for identification of rheological models of materials subjected to plastic deformation. *Archives of Civil and Mechanical Engineering*, *7*(1), 35–52. https://doi.org/https://doi.org/10.1016/S1644-9665(12)60003-X

Thomas, A. E., Abbes, B., Li, Y. M., Abbes, F., Guo, Y.-Q., & Duval, J.-L. (2017). A coupled thermo-mechanical pseudo inverse approach for preform design in forging. *AIP Conference Proceedings*, *1896*, 170004. https://doi.org/10.1063/1.5008202

Tiernan, P., & Hillery, M. T. (2004). Dieless wire drawing—an experimental and numerical analysis. *Journal of Materials Processing Tech.*, *155–156*(Complete), 1178–1183. https://doi.org/10.1016/j.jmatprotec.2004.04.175

Tiernan, P., & Hillery, M. T. (2008). Technical paper. *Journal of Manufacturing Processes*, *10*(1), 12–20. https://doi.org/10.1016/j.manpro.2008.05.001